Journal of Molecular Liquids 283 (2019) 804–815

Contents lists available at ScienceDirect

Journal of Molecular Liquids

journal homepage: www.elsevier.com/locate/molliq

Efficient estimation of CO_2 solubility in aqueous salt solutions

Mojtaba Raji [a], Amir Dashti [b,*], Pouria Amani [c], Amir H. Mohammadi [d,e,*]

[a] Separation Processes Research Group (SPRG), Department of Engineering, University of Kashan, Kashan, Iran
[b] Young Researchers and Elites Club, Science and Research Branch, Islamic Azad University, Tehran, Iran
[c] School of Chemical Engineering, University of Tehran, Tehran, Iran
[d] Institut de Recherche en Génie Chimique et Pétrolier (IRGCP), Paris Cedex, France
[e] Discipline of Chemical Engineering, School of Engineering, University of KwaZulu-Natal, Howard College Campus, King George V Avenue, Durban 4041, South Africa

ARTICLE INFO

Article history:
Received 8 December 2018
Received in revised form 18 February 2019
Accepted 19 February 2019
Available online 20 February 2019

Keywords:
CO_2 capture and sequestration
Salt solution
Brine
Modeling
Artificial intelligence

ABSTRACT

Industrialization and modernization have led to an increasing trend of greenhouse gas emissions entering the atmosphere. Consequently, many countries are imposing strict environmental regulations due to increasing concern on the climate change, and a significant amount of research is being conducted to tackle this problem. Carbon capture and sequestration are one of the major methods, which can remarkably contribute to this issue since a major greenhouse gas in Earth's atmosphere is carbon dioxide (CO_2). The general objective of this work was to investigate the significance of potential use of aqueous salt solutions for capturing CO_2 by developing an accurate model for estimation of this phenomenon. In particular, 608 experimental data of CO_2 solubility in aqueous solutions of salts as a function of temperature, pressure, salt solution concentration (molality), hydrogen bond acceptor count of salts, molecular weight of salts, and complexity value of the salts were collected from the literature. Four state-of-the-art computational methods (LSSVM, ANN, PSO-ANFIS and GA-ANFIS) were employed to examine their predictive capability for the problem. The results reveal that the LSSVM offers the highest accuracy with $R^2 = 0.9927$ and %AARD = 5.37. Although the neural network and fuzzy interface systems are more complex approaches, the superiority of the LSSVM method for the problem under study demonstrates the easy nature of this phenomenon. Thus, the LSSVM model is recommended for estimating the CO_2 solubility in aqueous salt solutions because not only it has more accuracy, but also it is easy to apply, has less mathematically complicated and less time-consuming.

© 2019 Published by Elsevier B.V.

1. Introduction

Current ascending trends of carbon dioxide (CO_2) entering the atmosphere has raised significant attention to develop and improve methods for reducing these emissions which can dramatically impact the environment, causing climate change for instance. A major area in this case is CO_2 capture and sequestration (CCS) [1–4]. Nowadays, many researchers are willing to promote new methods for separation and capture of CO_2 [5,6] and various techniques such as membrane separation process, pressure swing adsorption, chemical absorption and cryogenic technique have been investigated [7–11].

Various media are known to have the potential of capturing CO_2 inside their structure, among which saline aquifers (deep saline formations – mainly containing Na^+, K^+, Mg^{2+}, Ca^{2+}, Cl^- and SO_4^{-2}) are the most widely used due to their vast distribution [12]. To be more specific, four mechanisms are presented to demonstrate the way CO_2 is trapped inside saline formations: mineral trapping, solubility trapping, capillary trapping, and structural trapping [13,14]. The solubility trapping is known as the major mechanism responsible for 20% CO_2 distributing inside the formations [15].

It is clear that the CO_2 solubility in electrolyte solutions and saline formations is of significant importance and can potentially lead to various contributions not only in CCS but also in other applications such as CO_2-enhanced oil recovery [16–18], fluid inclusions [19,20], and CO_2-enhanced geothermal system [21–23]. Focusing on the investigations conducted on CO_2 solubility in aqueous electrolyte solutions, there are many studies examining the capacity of single-salt aqueous NaCl solutions for CO_2 capture, covering a wide range of temperature from 273 to 673 K and pressure from 0.1 to 150 MPa [19,24,25]. However, other salinities such as KCl, $MgCl_2$, Na_2SO_4, and $CaCl_2$ have received much less attention. Note that these salts are the most frequently encountered salt species in the aqueous environment including natural brines, seawater and groundwater [26,27]. Thus it is necessary to have enough experimental data and reliable models for CO_2 solubility in such CO_2-salt-H_2O systems.

Mathematical modeling and simulation methods are important tools in studying various processes in science and engineering [28–33]. Advanced mathematical tools are used for various purposes such as

* Corresponding authors.
E-mail addresses: amirdashti13681990@gmail.com (A. Dashti), a.h.m@irgcp.fr, amir_h_mohammadi@yahoo.com (A.H. Mohammadi).

https://doi.org/10.1016/j.molliq.2019.02.090
0167-7322/© 2019 Published by Elsevier B.V.

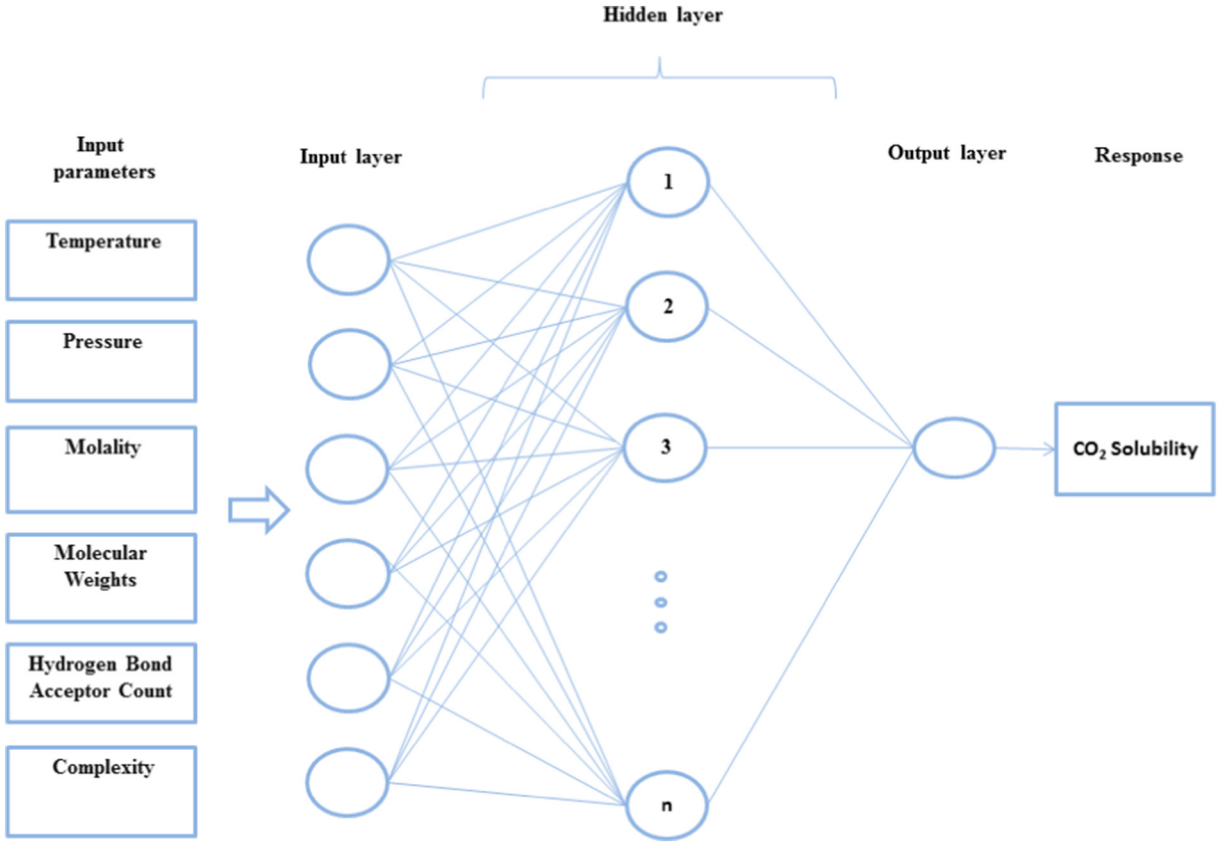

Fig. 1. Schematic of the MLP-ANN used in this study.

process development, identification, simulation and modeling, optimization, control, classification, clustering, forecasting, and monitoring [34].

This work focuses on the modeling the CO_2 solubility in salt solutions since development of a reliable model is vital for various industrial and commercial purposes. In the literature, there are extensive experimental studies on CO_2 solubility in aqueous salt solutions. There is a reasonable agreement between data of different researchers, while a few inconsistency exists in the reported data. For instance, the results of several articles [35–40] were compared and it was seen that there is a significant deviation between some data of Eremina et al. [41] at 298.15 K and 1 atm with $CaCl_2$ molality >0.015 mol.kg^{-1} and that reported by Onda et al. and Yashunishi et al. [35,36]. A part of data reported by Onda et al. [35] is inconsistent with Yasunish and Yoshida [36] and even with their own other data. The data of He and Morse [39] above 323.15 K have large deviations from other researchers' data. Malinin and Savelyeva [37] and Malinin and Kurovskaya [38] reported different solubility values at several same conditions. Neglecting all these inconsistencies, a wide range of reliable experimental data of CO_2 solubility in $CaCl_2$ solutions was gathered covering the temperature range of 273.15 to 424.64 K, pressure range of 0.98 to 712.31 bar, and concentration range of 0.002 to 6.30 mol.kg^{-1}. However, there are limited investigations on CO_2 solubility in such solutions, covering a narrow range of conditions. Thus, currently these data are not adequate to be used for developing a reliable model.

Surveying a number of extensive efforts to model the CO_2 solubility in pure water and aqueous electrolyte solutions, several models are currently available for aqueous solution solutions [24,42–45]. However, each of these models have their own limitations and drawbacks. For instance, the maximum pressure for the system in the model of Sørensen et al. [42] is 1.8 bar, while it is far below the conditions in CCS. Moreover, the average deviation of CO_2 solubility is about 17% which can be considered as an inacceptable error. In another example, although the model of Duan et al. [43,44] is applicable for both single and mixed-salt solutions, the deviation of the prediction is significant. Marin and Patroescu [45] and Zhao et al. [24] presented a semi-empirical model and a fugacity-activity model for several aqueous electrolyte solutions. Considering all these efforts, it is highly essential to examine the state-of-the-art computational methods in this case since many conventional approaches are complex, costly, and time consuming.

Table 1
Layers of an ANFIS model.

Layer	Task	equation	Notes
1st	Fuzzification	$Q_{1,i} = \mu_{\alpha_i}(x)\ \ i = 1,2$ $Q_{1,i} = \mu_{\beta_{(i-2)}}(y)\ \ i = 3,4$	μ_α and μ_β are the fuzzy membership functions.
2nd	Rule layer	$O_{2,i} = W_i = \mu_{A_i}(x)\mu_{B_i}(x)$	The output is the consequence product of all inletting signals.
3rd	Normalization	$O_{3,i} = \overline{w_i} = \frac{w_i}{w_1 + w_2}, i = 1,2$	The normalized firing strength is computed in this layer.
4th	Defuzzification	$O_{4,i=}\overline{w_i} f_i = \overline{w_i}(p_i x + q_i y + r_i)$ for $i = 1,2$	Each node i has an adaptive relation with a node function:
5th	Output	$O_{5,i=} \sum_i \overline{w_i} f_i = \frac{\sum_i w_i f_i}{\sum_i w_i}$ for $i = 1,2$	The total output is computed by summation of all incoming signals.

Table 2
Information of the data used in this study.

Pressure (MPa)	Temperature (K)	Molality (Mol/kg)	Complexity	Molecular weight	Hydrogen bond acceptor count	Solubility (mol fraction)	References
1.519875 - 88.55805	323–423	0.333–3.898	0	110.978($CaCl_2$)	2	0.0003–0.022	[70,71]
0.00651–18.215	313.1–433.1	0.5–4.05	2	74.548 (KCl)	1	0–0.02174	[72–74]
0.0192 −15	286.97–433.16	0.249711−2.01	62.2	142.046(Na_2So_4)	4	0–0.034778	[70,75,76]

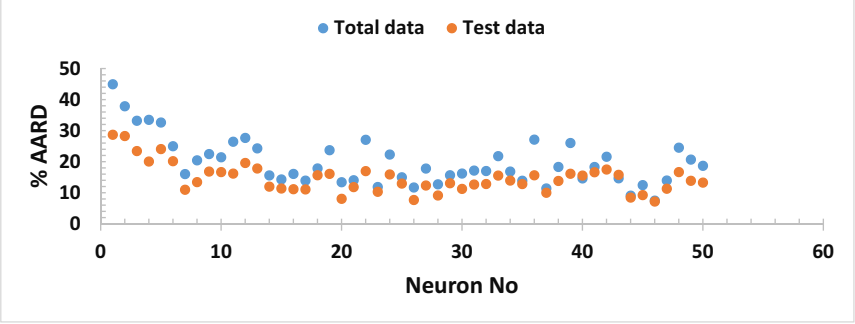

Fig. 2. %AARD of test and total data in ANN model vs. number of neuron

In this work, artificial neural network (ANN), adaptive network-based fuzzy inference system (ANFIS), and support vector machines (SVM) were employed to tackle the problem. The performances of these models were optimized using the most expert optimization techniques including particle optimization swarm (PSO), genetic algorithm (GA), and coupled simulated annealing (CSA). The results of this work not only give a general idea of the complexity of the problem, but also can be very helpful for industrial purposes where the accuracy of the calculations is of fundamental importance. The novelty of this work is the introduction of the new descriptors or parameters in the AI modeling of the CO_2 solubility in aqueous salts solution. The methods introduced in this work can be a guideline for further researches regarding AI modeling of gas solubility in various materials or compounds. Besides, for the first time, AI modeling of CO_2 solubility in several aqueous salt solution by single models is presented.

2. Modeling framework

2.1. MLP-ANN approach

Artificial intelligence (AI) systems are fit to gain experience and improve the execution and adaptation to alterations in the environment [46]. These systems are designed to handle large amount of data regarding the achievement of a conclusion. An MLP network comprises of three different layers (i.e., input, output and hidden layers), as shown in Fig. 1. Each hidden layer consists of one or several neurons, which can lead to different prediction capabilities. Thus, there is a need for an intelligent approach or any trial and error method to optimize the number of layers and neurons for reaching the optimum performance.

Table 3
Information for the PSO-ANFIS model developed in this study.

Parameter	Value
Maximum iterations number	1000
Maximum particles number	200
Initial inertia weight (W_{min})	0.5
Inertia weight damping ratio (W_{damp})	0.99
Cognitive acceleration (C_1)	1
Social acceleration (C_2)	2
Number of fuzzy rules	10

Commonly, mean square error is used to represent the execution of developed networks [47]. In a MLP network, the gradient descent (backpropagation - BP) is employed to supervise the learning procedure. The number of training steps (i.e., epochs) is also very important to avoid under training in which the learning cannot be accomplished, and over training which leads to remembering rather than learning, thereby poor execution of the network [48].

2.2. ANFIS approach

A typical ANFIS model is based on first-order Takagi–Sugeno Inference. Considering x and y as inputs and f as the output, fuzzy *if–then* rules are expressed as [49]:

Rule 1:

$$\textbf{If } x \text{ is } \alpha_1 \text{and } y \text{ is } \beta_1; \textbf{then } f1 = m_1x + n_1y + r_1 \quad (1)$$

Rule 2:

$$\textbf{If } x \text{ is } \alpha_2 \text{and } y \text{ is } \beta_2; \textbf{then } f2 = m_2x + n_2y + r_2 \quad (2)$$

in which, α and β represent the fuzzy sets for x and y, respectively. Also, m, n, and r are the coefficients of the output function being determined through training process.

Any ANFIS structure comprises of five different layers. An introduction on each of these layers and their corresponding roles is given in Table 1.

Table 4
Information for the GA-ANFIS model developed in this study.

Parameter	Value
Population size	30
Maximum number of generation in GA	1000
Mutation percentage in GA	0.7
Crossover percentage	0.65
Mutation rate	0.05
Number of fuzzy rules	10

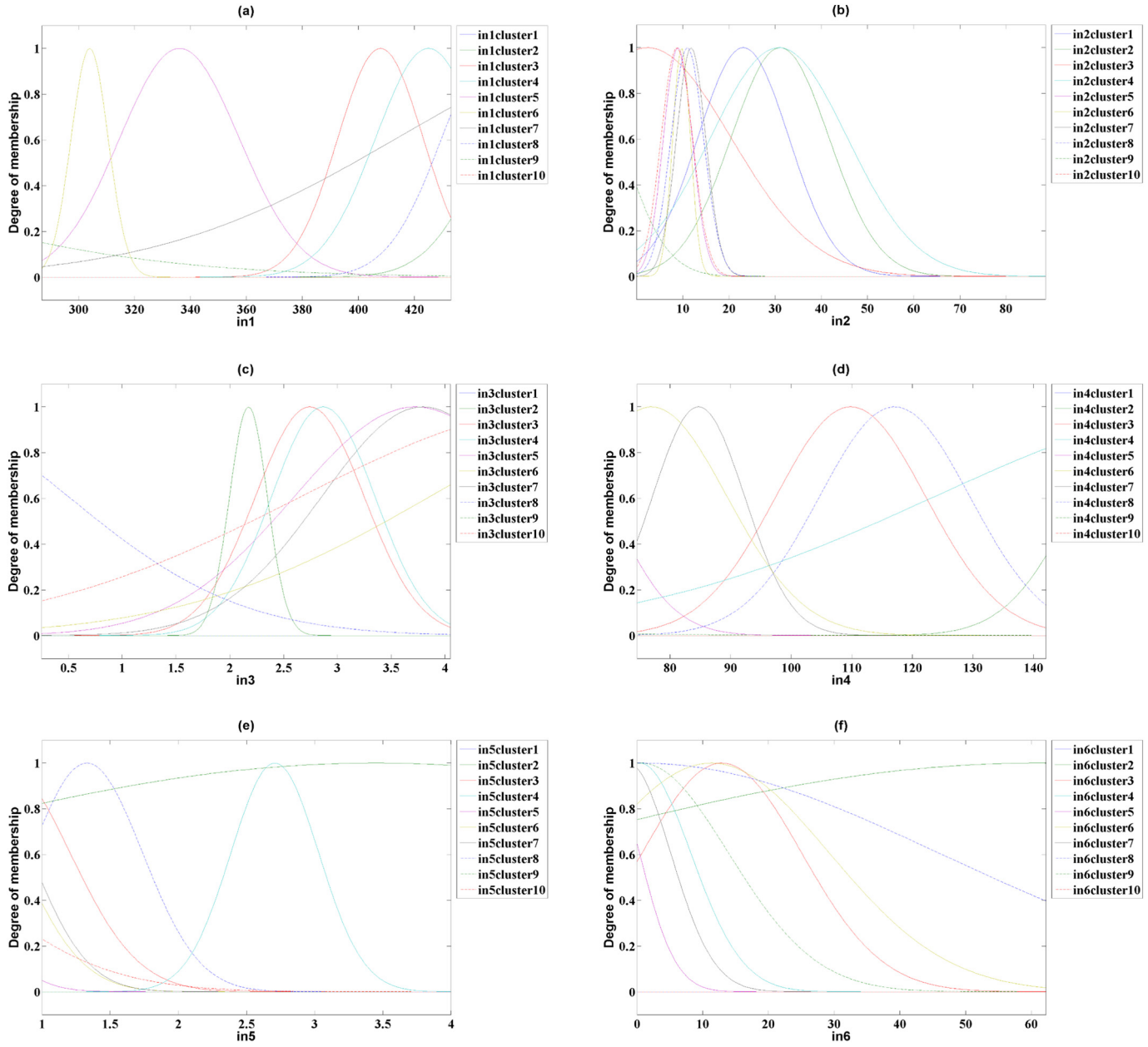

Fig. 3. The MFs for (a) temperature, (b) pressure, (c) solution concentration, (d) hydrogen bond acceptor count of salts, (e) molecular weight of salts, and (f) complexity value of salts for the PSO-ANFIS model.

2.3. LSSVM approach

Vapnik [50] was the first person who introduced the SVM as a superior improvement in AI systems. It is capable of solving both regression and classification problems, but it has one drawback: a high amount of quadratic programming problems is needed to be solved through computing procedures. This issue is addressed by involving the linear equations rather than quadratic programming which is known as the Least Squares SVM (LSSVM), thereby simplifying the optimizing procedure [51]. Based on a presumed data set $(x_i, y_i)_n$, the regression with LSSVM is employed to prognosticate a function in which x_i, y_i, and n stand for the input, target and the number of data to be trained [52,53].

Eq. (3) expresses the regression function of the SVM, where $\varnothing(x)$ and w stand for the nonlinear function and weight vector [54]:

$$f(x) = w^T \varnothing(x_k) + b \tag{3}$$

Note that $\varnothing(x)$ can be of sigmoid, radial basis, polynomial, or linear form. The values of w and b can be optimized by minimization of the empirical risk along with considering a complexity term as below [55]:

$$min \frac{1}{2}\|\omega^2\| + C\sum_{i=1}^{n}(\xi_i - \xi_i^*) \tag{4}$$

$$\begin{aligned} &y_k - w^T\varnothing(x_k) - b \le \varepsilon + \xi_k, \quad k = 1, \ldots, N \\ &\{w^T\varnothing(x_k) + b - y_k \le \varepsilon + \xi_k^*, \quad k = 1, \ldots, N \\ &\xi_k, \xi_k^* \ge 0 \quad k = 1, \ldots, N \end{aligned} \tag{5}$$

The ε-insensitive loss function is as follows:

$$L_e(f(x_i), y_i) = \begin{cases} 0 \; for \; |f(x_i) - y_i| < \varepsilon \\ |f(x_i) - y_i| - \varepsilon \; otherwise \end{cases} \tag{6}$$

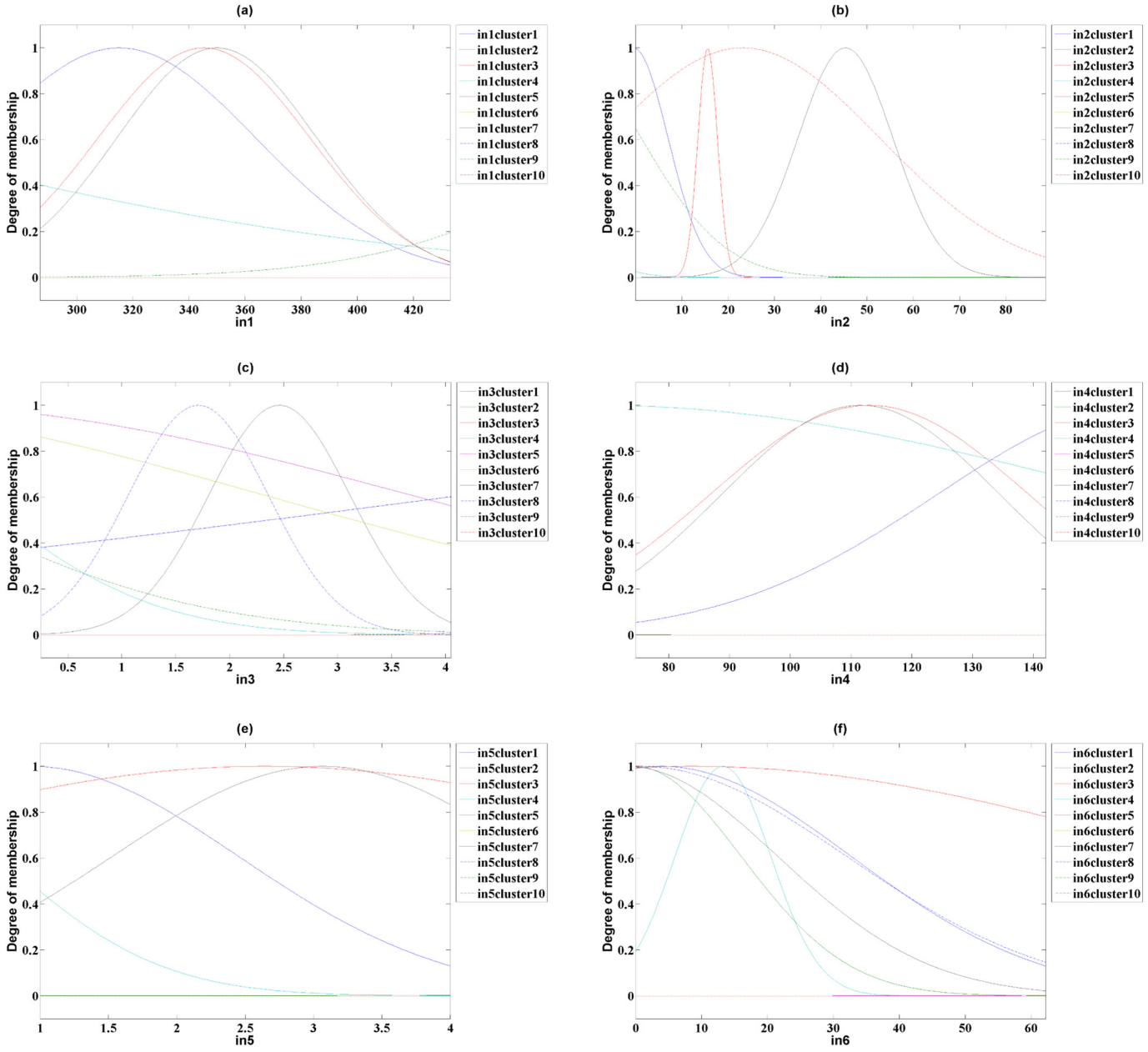

Fig. 4. The MFs for (a) temperature, (b) pressure, (c) solution concentration, (d) hydrogen bond acceptor count of salts, (e) molecular weight of salts, and (f) complexity value of salts for the GA-ANFIS model.

Considering the limitations (Eq. (6)) into the optimization (Eq. (5)), the saddle point of Lagrangian is derived as follows:

$$\begin{aligned} L_{SVM} &= \frac{1}{2}\|\omega\|^2 + C\sum_{i=1}^{n}(\xi_k - \xi_k^*) \\ &- \sum_{i=1}^{n}\alpha_i(\varepsilon_i + \xi_k - y_i + \langle\omega, \varnothing(x_i)\rangle + b) \\ &- \sum_{i=1}^{n}\alpha_i^*(\varepsilon_i + \xi_k^* - y_i - \langle\omega, \varnothing(x_i)\rangle - b) \\ &- \sum_{i=1}^{n}(\eta_i\xi_k - \eta_i^*\xi_k^*) \end{aligned} \tag{7}$$

where η_i, ξ_k, ξ_k^*, $\eta_i^*$are the Lagrange multipliers. Next, by differentiating Eq. (7) with respect to ω, b, ξ_k, ξ_k^* the following set of terminate equations is attained:

$$\begin{aligned} &\frac{\partial L_{SVM}}{\partial w} = 0 \rightarrow w = \sum_{k=1}^{N}(\alpha_i - \alpha_i^*)\varnothing(x_i) \\ &\frac{\partial L_{SVM}}{\partial b} = 0 \rightarrow \sum_{k=1}^{N}(\alpha_i - \alpha_i^*) = 0 \\ &\frac{\partial L_{SVM}}{\partial e_i} = 0 \rightarrow C - \alpha_i - \eta_i = 0 \\ &\frac{\partial L_{SVM}}{\partial \alpha_i} = 0 \rightarrow C - \alpha_i - \eta_i = 0 \end{aligned} \tag{8}$$

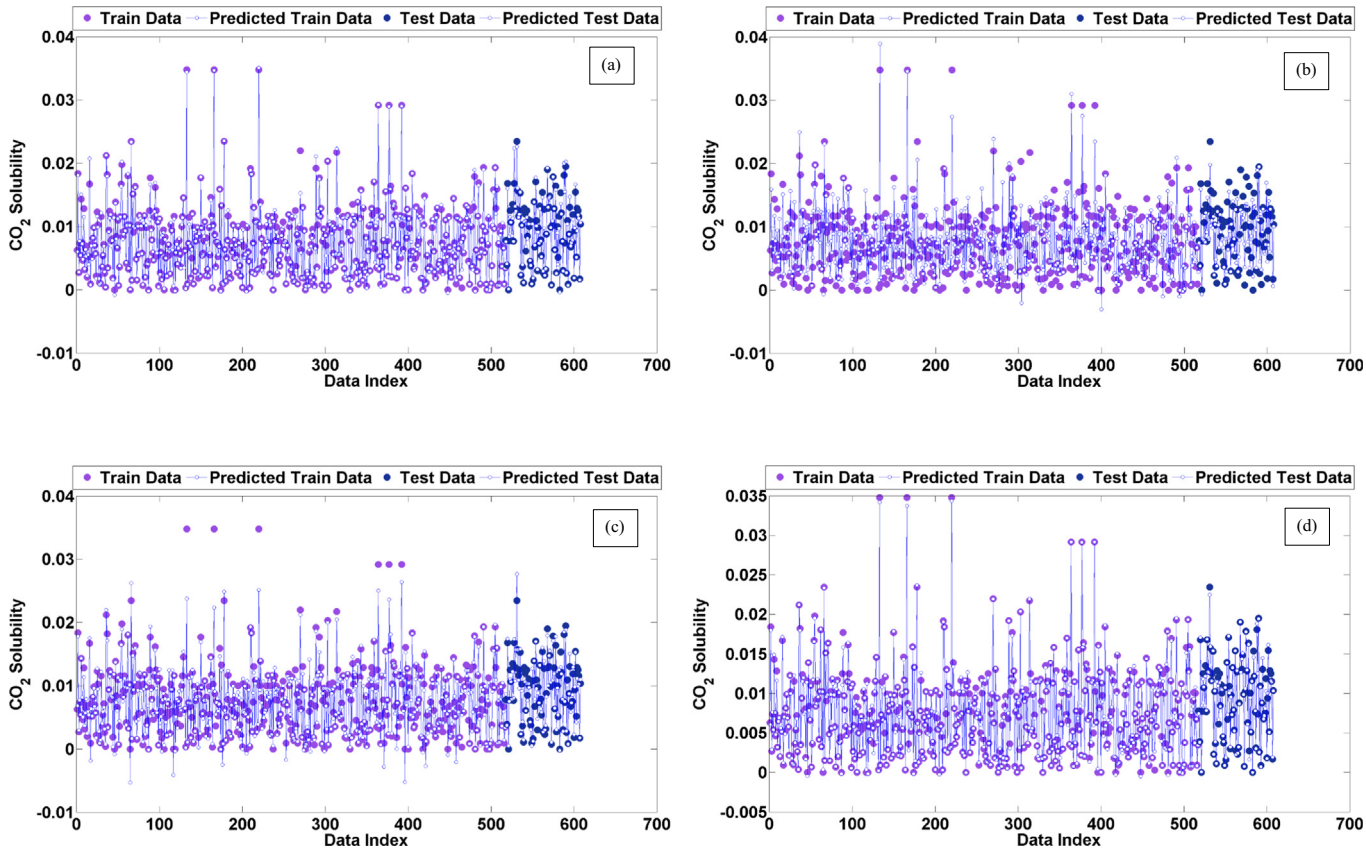

Fig. 5. Actual CO_2 solubility versus estimated data at testing and training stages for (a) ANN, (b) GA-ANFIS, (c) PSO-ANFIS and (d) LSSVM.

Furthermore, from the optimization conditions, a dual problem is obtained as below:

$$\begin{aligned}\underset{(a,a^*)}{Max}(Q) = &-\frac{1}{2}\sum_{i,j=1}\left(\alpha_i-\alpha_j^*\right)\\ &\times\left(\alpha_j-\alpha_j^*\right)\prec\varnothing(x_i),\varnothing(x_j)\succ-\varepsilon\sum_{i=1}^{n}(\alpha_i-\alpha_i^*)\\ &+\sum_{i=1}^{n}y_i(\alpha_i+\alpha_i^*)\end{aligned} \tag{9}$$

$$S.t.\{\ \sum_{i=1}^{n}(\alpha_i-\alpha_i^*)=0\}\quad \alpha_i,\ \ \alpha_i^*\in[0,C] \tag{10}$$

Therefore, the SVM problem is expressed as [56]:

$$fx=(\sum_{i=1}^{n}\alpha_i-\alpha_i^*K(x,x_i)+b \tag{11}$$

where $K(x_i,x_j)=\varnothing(x_i)^T\varnothing(x_j)$ is the mapped kernel into every processes.

As mentioned earlier, LSSVM offers much more simplicity in calculations by dealing with linear sets of equations rather than inequality limitations. The function approximation in the LS-SVM is expressed as:

$$\begin{aligned}&\underset{\omega,b,e}{min}J(\omega,e)=\frac{1}{2}\|\omega\|^2+\frac{1}{2}\gamma\sum_{i=1}^{n}e_i^2\\ &\text{S.T.}y_i=\langle\omega,\varnothing(x_i)\rangle+b+e_i\end{aligned} \tag{12}$$

where γ and e_i are the regularization and the error values, respectively. In addition, the Lagrangian is calculated as below [57]:

$$L_{LSSVM}=\frac{1}{2}\|\omega\|^2+\frac{1}{2}\gamma\sum_{i=1}^{N}e_i^2-\sum_{i=1}^{N}\alpha_i\{(\omega,\varnothing x_i)+b+e_i-y_i\} \tag{13}$$

where α_i is the Lagrange multiplier. Accordingly, the optimization problem is solved by LS-SVM as follows:

$$\begin{aligned}&\frac{\partial L_{LSSVM}}{\partial w}=0\rightarrow w=\sum_{i-1}^{N}\alpha_i\varnothing(x_i)\\ &\frac{\partial L_{LSSVM}}{\partial b}=0\rightarrow\sum_{i-1}^{N}\alpha_i=0\\ &\frac{\partial L_{LSSVM}}{\partial e_i}=0\rightarrow\alpha_k=\gamma e_i i=1,2,\ldots,N\\ &\frac{\partial L_{LSSVM}}{\partial\alpha_i}=0\rightarrow(w.\varnothing(x_i))+e_i+b-y_i=0,i=1,2,\ldots.,N\end{aligned} \tag{14}$$

By eliminating ω and e_i, and introducing $Y=[y_1,\ldots,y_n]$, $1_v=[1,\ldots,l]$, and $\alpha=[\alpha_1,\ldots,\alpha_n]$, we have [51]:

$$\begin{bmatrix}0 & l_n^T\\ l_v & \Omega+\gamma^{-1}l_n\end{bmatrix}\begin{bmatrix}b\\ \alpha\end{bmatrix}=\begin{bmatrix}0\\ Y\end{bmatrix} \tag{15}$$

where Ω and l_v denote the kernel and identity matrix. Ω is derived as:

$$\Omega_{ij}=\varnothing(x_i)\varnothing(x_j)=K(x_i.x_l) \tag{16}$$

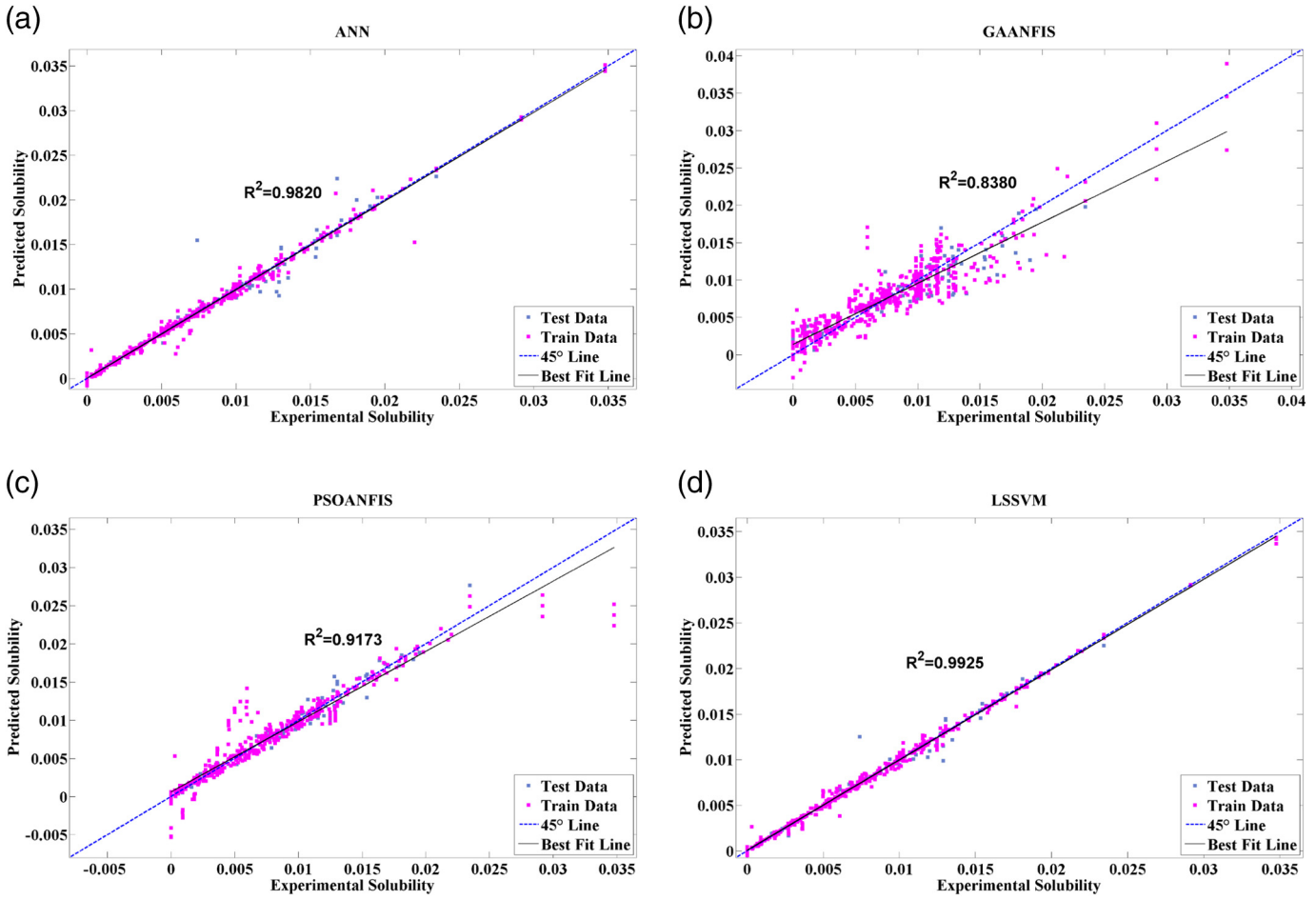

Fig. 6. Regression plot for the solubility of CO_2 prognostication by (a) ANN, (b) GA-ANFIS, (c) PSO-ANFIS and (d) LSSVM.

Note that various types of kernel functions are employed in the LSSVM such as sigmoid, polynomial, radial basis, polynomial, and linear [57]. However, radial basis and polynomial are the most commonly used functions, respectively expressed as:

$$K(x_i, x_j) = \left(1 + \frac{x_i^T x_j}{C}\right)^d \tag{17}$$

$$\mathrm{k}(x_i, \mathrm{x_j}) = \exp\left(\frac{-\|\mathrm{x_i} - x_j\|^2}{\sigma^2}\right) \tag{18}$$

In this study, radial basis function (Eq. (17)) was used due to its acceptable application. Accordingly, there are two adjustable parameters (γ and σ^2) in the problem under study, which show the superiority of this approach over other computational methods such as ANN.

2.4. PSO algorithm

The PSO was introduced by Kennedy and Eberhart [58,59] inspired from natural swarm and flock of insects and birds. The PSO finds the optimal solution based on generating a population of random solutions and then updating generation. In this method, "particle" is referred as the potential solutions. In fact, all particles go through the problem space owing their own position and velocity. This algorithm tries to find the best positions with good fitness for particles by tracking two objectives: (I) the best position for each particle (p_{best}) and its global value (g_{best}) [60]. Therefore, in every iteration, the obtained solution is compared to these two values.

The new position of particles is determined as below:

$$v_i(t+1) = w.v_i(t) + c_1.\ rand_1.(pbest_i(t) - x_i(t)) + c_2.\ rand_2(gbest_i(t) - x_i(t)) \tag{19}$$

$$x_i(t+1) = x_i(t) + v_i(t+1), i = 1 \ldots \mathrm{N} \tag{20}$$

where x and v are position and velocity of particles, N indicates the quantity of particles, c_1 and c_2 denote the relative impact of the social and cognitive components (i.e., learning factors), and w denotes inertia weight controlling the influence of previous velocity of a particle on its new velocity. Moreover, $rand_1$ and $rand_2$ are random numbers between 0 and 1.

2.5. GA algorithm

The GA is another optimization method which is inspired from the nature. The optimization or in other words, the evolutionary computation was developed on the basis of Weismann, Darwin's theory [61], evolutionary process [62], and genetics of Mendel [63]. In fact, randomly and simultaneously identifying many routs and finding a different zone in the special area are the vital features of GA [64,65]. Moreover, its initial operators are mutation, crossover, and inversion which are responsible for conserving the balance between explorations for finding new zones and exploitation in formation [66]. The GA first constructs an initial population after determining a problem. Then, the objective function considers the originality of each solution. The population is classified at the next step, based on fitness of individuals (known as "particles" in PSO approach). Then, crossover and mutation are

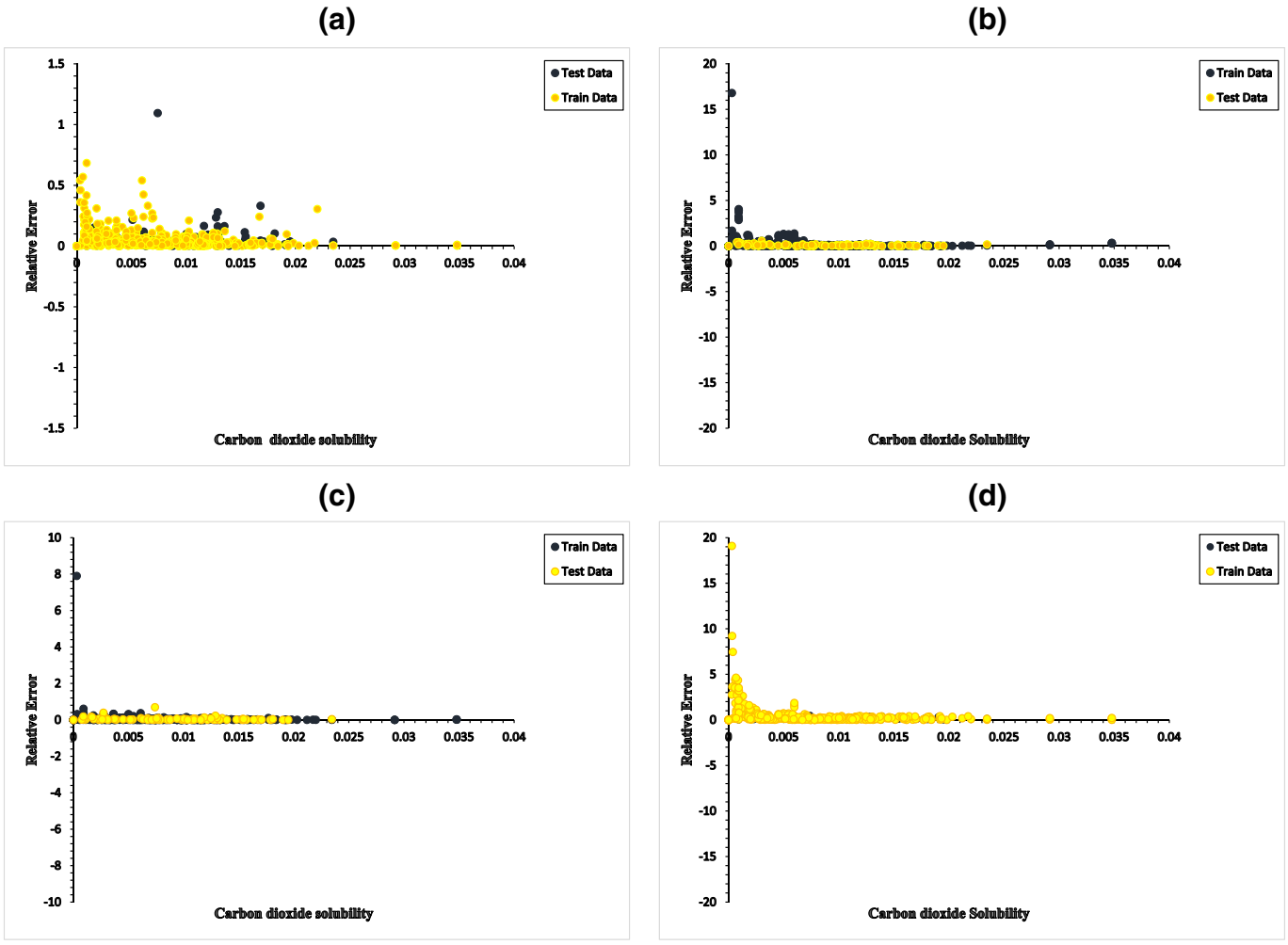

Fig. 7. Relative deviation of the estimated CO_2 solubility values for both test and train data points by (a) ANN, (b) GA-ANFIS, (c) PSO-ANFIS and (d) LSSVM.

considered on the proper individual to create the next generation, continuing till the fulfillment of the ending criteria is achieved.

2.6. CSA algorithm

SA is a computational method which allows to move to solutions with poorer qualities regarding the expedition in escaping from local optima, while its probability is reduced during the procedure [67]. The CSA is developed to improve the acceptance probability and to ease the getting away process from local optima in non-convex problems. In this way, the optimization accuracy was found to be significantly increased by coupling involving local optimization processes, along with a very small decrease in the convergence pace [68]. A detailed description of how the CSA algorithm works is given in Ref. [69].

3. Results and discussion

The development of an accurate and reliable approach to model and predict a problem is always of significant interest. In this work, it was intended to propose and develop a proper method to estimate the CO_2 solubility in KCl, Na_2SO_4 and $CaCl_2$ aqueous solutions which can be very beneficial in CO_2-enhanced oil recovery and geothermal systems. Here, 608 experimental data of CO_2 solubility (x_{CO2}) were taken from literature at different temperatures (K), pressures (MPa), molality and its mole fraction (x_{Salt}). The statistical details of the considered data is given in Table 2.

In the following, LSSVM, ANN, PSO-ANFIS and GA-ANFIS were used to model the problem under study.

Four different error functions employed to determine the predictive capability of models, including correlation factor (R^2), Average Absolute Relative Error (AARD), Standard Deviation (STD), and Mean Square Error (MSE). These statistical functions are given below, respectively.

$$R^2 = 1 - \frac{\sum_{i=1}^{n}\left[x_i^{sim} - x_i^{exp}\right]}{\sum_{i=1}^{n}\left[x_i^{sim} - x^m\right]}, x_m = \frac{\sum_{i=1}^{n} x_i^{sim}}{n} \tag{21}$$

$$\%AARD = \frac{100}{N}\sum_{i=1}^{n}\left|\frac{x_i^{sim} - x_i^{exp}}{x_i^{exp}}\right| \tag{22}$$

$$STD = \sum_{i=1}^{n}\left(\frac{\left(x_i^{sim} - x_m\right)^2}{N}\right)^{0.5} \tag{23}$$

$$MSE = \frac{1}{n}\sum_{i=1}^{n}\left(x_i^{exp} - x_i^{sim}\right)^2 \tag{24}$$

In the above equations, x_i^{exp} and x_i^{sim} denote the actual and the prognosticated values, respectively; n is the number of experimental data.

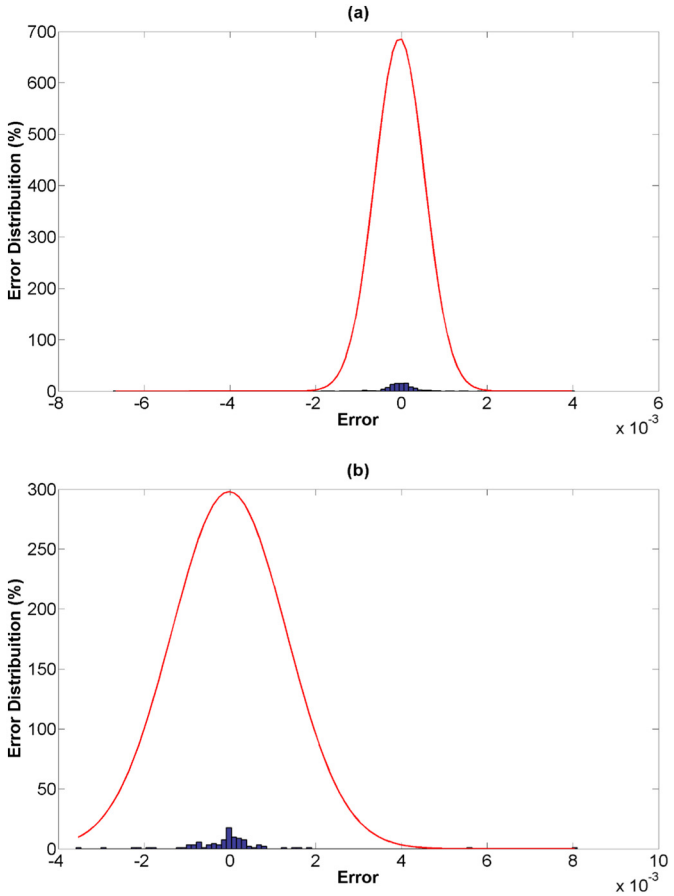

Fig. 8. Histogram of errors for the ANN model at (a) training and (b) testing stages.

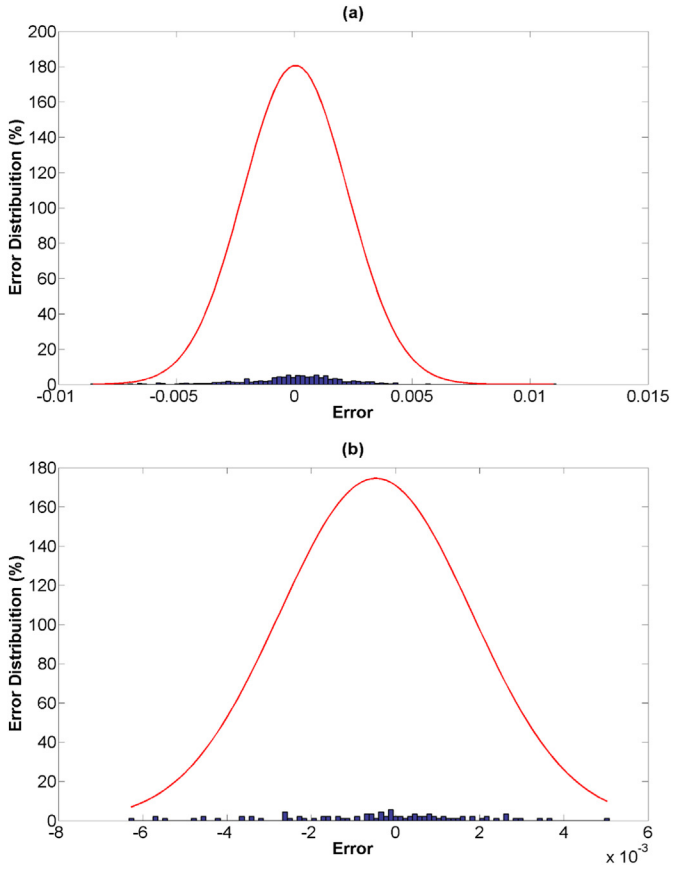

Fig. 9. Histogram of errors for the GA-ANFIS model at (a) training and (b) testing stages.

3.1. ANN performance

For a proper development of an ANN, its structure needs to be optimized based on the number of hidden layers and the quantity of neurons in each of the layers. For this purpose, *logsig* and *purelin* transfer functions were employed to treat the hidden and output layers. Different configurations were tested and their performances were compared using the error %AARD. Among BP methods, the Levenberg-Marquardt (LM) was used to adjust the weights and to train the network since its superb capability of training the network is provided in the literature [77].

Accordingly, networks of different structures were developed and tested. The comparative performance of different networks is presented in Fig. 2, indicating the achievement of the best results using 46 neurons. In the 46th neuron lowest %AARD was observed for test and total data.

3.2. ANFIS performance optimized with GA and PSO

The implementation of an optimization algorithm in an ANFIS based model can significantly boost the predictive capacity of the model. Here, PSO and GA algorithms were applied for optimizing the training procedure of the ANFIS.

Regarding the development of a PSO-ANFIS model, various parametric studies were conducted to find and set the optimum PSO parameters for the problem under study. In general, the PSO algorithm is a hybrid model owning closer relationship between input and output data. Thus, it can significantly improve tackling the non-linear problems. Here, the membership function (MF) used in the model was the Gaussian, due to its superior contribution seen in the literature [47,78–82]. In addition, the trial-and-error approach was used to find the optimum values for the given parameters. Table 3 presents the procedure of finding the optimum values of PSO parameters.

Regarding the development of a GA-ANFIS model, Gaussian MF was used similar to PSO-ANFIS. Its code is run with MATLAB package. Again, same as the procedure for PSO-ANFIS, several key GA parameters were considered to be optimized to achieve the best results. The trial-and-error method was used to keep track of model performance of different GA parameters. These parameters and the performance of the model using different values of these parameters are given in Table 4.

Furthermore, to better understanding the PSO- and GA-ANFIS structures, schematic presentation of the MFs are provided in Figs. 3 and 4, respectively.

3.3. LSSVM performance optimized with CSA

As it was aforementioned, for developing the best network of the LS-SVM model, γ and σ^2 are needed to be determined. Here, the CSA was employed for this purpose; finding the optimum values of γ and σ^2. The results revealed that if $\gamma = 3209.8810$ and $\sigma^2 = 1.2464$, the most accurate estimation of the considered data can be achieved.

3.4. Finding the superior model

Regarding the comprehensive comparison between the performances of developed models, various statistical error functions and different graphical approaches were conducted. First presentation is the direct comparison between the actual data of experiments and predicted results from each model. It is given in Fig. 5. From the figure, one can see that all developed networks are satisfactorily able to provide an accurate estimation. Very good overlapping between actual

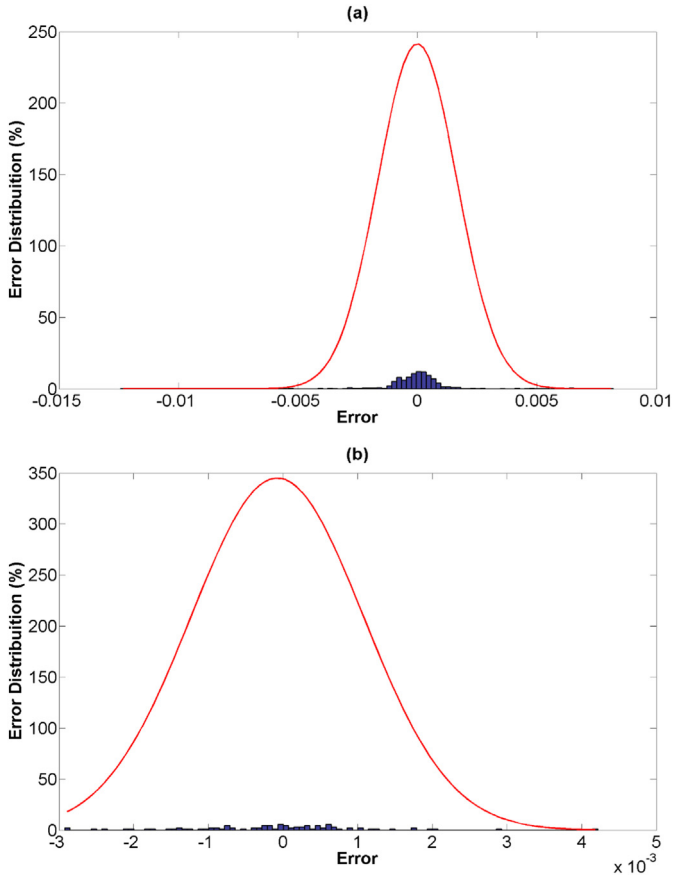

Fig. 10. Histogram of errors for the PSO-ANFIS model at (a) training and (b) testing stages.

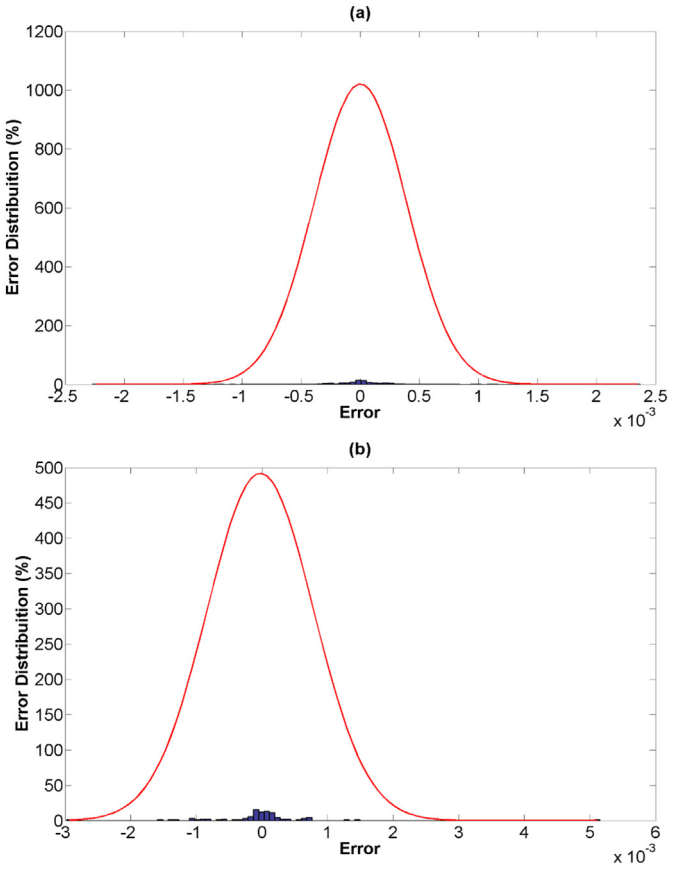

Fig. 11. Histogram of errors for the LSSVM model at (a) training and (b) testing stages.

and estimated data can be observed from the figures, indicating the capability of models to find and follow the pattern of experimental data. In completion of Fig. 5, the corresponding regression values are given in Fig. 6 as well, indicating the very good estimation of the experimental data via four developed models. In fact, the R^2 of CSA-LSSVM, GA-ANFIS, MLP-ANN and PSO-ANFIS models are respectively 0.9925, 0.8380, 0.9810 and 0.9173. The good estimation of test data set indicates that no overtraining or undertraining is conducted.

Furthermore, Fig. 7 demonstrates the relative deviations of model outputs with respect to the target values, which can be very helpful to understand the comparative performance of models. Accordingly, more compacted relative deviations of the models' results is seen around the zero deviation line, showing high consistency between actual data and those estimated by the models. Furthermore, it is found that the LSSVM and ANN models perform better compared to the other models.

Plots of errors histograms for ANN, GA-ANFIS, PSO-ANFIS and LSSVM models are shown in Figs. 8–11.

As mentioned earlier, four different statistical functions including R^2, AARD%, STD, and MSE were considered to make a comparison between the predictive capability of developed models. Table 5 presents these values. The errors indicates that LSSVM has the highest precise. In addition to very high accuracy obtained using LSSVM, it has the highest speed for CO_2 solubility estimation while the convergence speed is of significant importance especially while treating big data. Furthermore, the LSSVM is a correlative method and it can be a strong tool to cover a wide range of input information.

3.5. Sensitivity analysis

A sensitivity analysis was conducted for examining the effect of individual input parameters on CO_2 solubility values. The relevancy factor (r) is used to achieve the relative influence of each input parameter, and to determine which inputs have the most effectiveness. The r value ranged from −1 to +1; the higher absolute value, the higher effectiveness. The strength of r values is calculated by [83]:

$$r = \frac{\sum_{i=1}^{n}(X_{k,i}-\overline{X_k})(Y_i-\overline{Y})}{\sqrt{\sum_{i=1}^{n}(X_{k,i}-\overline{X_k})^2\sum_{i=1}^{n}(Y_i-\overline{Y})^2}} \quad (25)$$

In Eq. (25), n is the number of data sets, Y_i and $\overline{Y}$ represent the 'i'th and average values of output, and $X_{k,i}$, and X_k represent the 'i'th and the average values of the kth input. The corresponding data for all data sets is shown in Fig. 12. It is seen in Fig. 12 that CO_2 solubility varies directly with respect to hydrogen bond acceptor counts and complexity, molecular weight, and pressure. On the other hand, it varies inversely as the molarity and temperature change. Among the considered inputs, it is found that the complexity and pressure have the least and most significant impact on CO_2 solubility. It can be concluded by relevancy factor results that by increasing the temperature and molality of the solution, the CO_2 solubility is decreased, besides, by increasing the pressure, the CO_2 solubility is increased.

4. Conclusion

This study investigates the performances of various state-of-the-art computational algorithms including MLP-ANN, GA-ANFIS, CSA-LSSVM, and PSO-ANFIS for the estimation of CO_2 solubility in aqueous salt solution. 608 experimental data of CO_2 solubility (x_{CO2}) from the literature were taken at different temperatures, pressures, salts concentration and its mole fraction (x_{Salt}). Several statistical functions and graphical representations were employed to quantitatively compare the accuracy of developed models. It was found that all models are acceptably able to

Table 5
Prediction accuracy of different models.

	ANN			LSSVM			PSO-ANFIS		GA-ANFIS		
	Train	Test	Total	Train	Test	Total	Train	Test	Total	Train	Test	Total
R^2	0.9890	0.9371	0.9820	0.9950	0.9759	0.9925	0.9106	0.9527	0.9173	0.8406	0.8142	0.8380
MSE	0.0000	0.0000	0.0000	0.0000	0.0000	0.0000	0.0000	0.0000	0.0000	0.0000	0.0000	0.0000
STD	0.0055	0.0053	0.0055	0.0055	0.0052	0.0055	0.0053	0.0053	0.0053	0.0050	0.0043	0.0049
%AARD	7.51	7.17	7.46	5.96	5.43	5.88	23.14	10.69	21.25	43.36	29.92	41.32

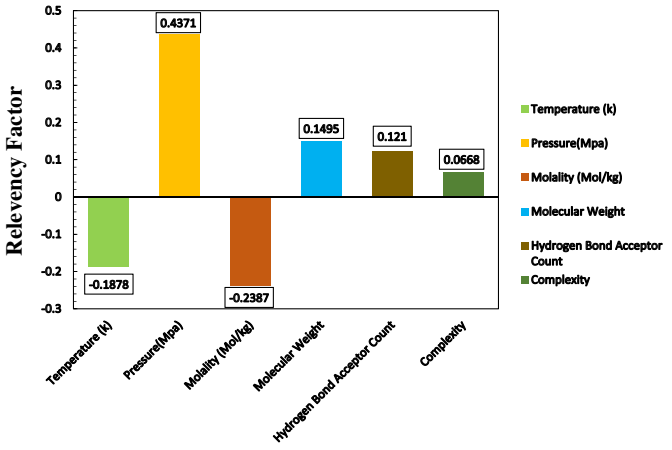

Fig. 12. Sensitivity analysis to find out the impact of input parameters on CO_2 solubility in salt.

provide an accurate estimation of experimental data. On one hand, very high values of R^2 (for CSA-LSSVM) indicate the easy nature of the problem under study; on the other hand, it indicates the potential use of AI methods for estimating the CO_2 solubility. Therefore, the LSSVM model is highly recommended for such problems for several reasons: (I) it has the highest accuracy, (II) it is an AI method and offers much higher speed for estimating the data (time can become significantly high while treating big data in other models); and (III) it is a correlative method and has higher capability of covering a wider range of input parameters. Overall, all these models are very suitable for such applications such as CO_2 absorption and gas processing where accurate estimation of CO_2 solubility is highly appreciated.

References

[1] M.E. Boot-Handford, J.C. Abanades, E.J. Anthony, M.J. Blunt, S. Brandani, N. Mac Dowell, J.R. Fernández, M.-C. Ferrari, R. Gross, J.P. Hallett, Energy Environ. Sci. 7 (2014) 130.
[2] V. Scott, S. Gilfillan, N. Markusson, H. Chalmers, R.S. Haszeldine, Nat. Clim. Chang. 3 (2013) 105.
[3] A. Dashti, M. Raji, A. Razmi, N. Rezaei, S. Zendehboudi, M. Asghari, Chem. Eng. Res. Des. (2019) (In press).
[4] M. Aghaie, N. Rezaei, S. Zendehboudi, J. Mol. Liq. 275 (2019) 323.
[5] S. Saeidi, N.A.S. Amin, M.R. Rahimpour, J. CO_2 Util. 5 (2014) 66.
[6] M.K. Mondal, H.K. Balsora, P. Varshney, Energy 46 (2012) 431.
[7] A.M. Yousef, W.M. El-Maghlany, Y.A. Eldrainy, A. Attia, Energy 156 (2018) 328.
[8] F.R. Abdeen, M. Mel, M.S. Jami, S.I. Ihsan, A.F. Ismail, Chin. J. Chem. Eng. 24 (2016) 693.
[9] R. Augelletti, M. Conti, M.C. Annesini, J. Clean. Prod. 140 (2017) 1390.
[10] G. Sodeifian, M. Raji, M. Asghari, M. Rezakazemi, A. Dashti, Chin. J. Chem. Eng. (2018) (In press).
[11] M. Aghaie, N. Rezaei, S. Zendehboudi, Renew. Sust. Energ. Rev. 96 (2018) 502.
[12] C.M. White, B.R. Strazisar, E.J. Granite, J.S. Hoffman, H.W. Pennline, J. Air Waste Manage. Assoc. 53 (2003) 645.
[13] S.M. Benson, D.R. Cole, Elements 4 (2008) 325.
[14] N.I. Gershenzon, R.W. Ritzi, D.F. Dominic, M. Soltanian, E. Mehnert, R.T. Okwen, Water Resour. Res. 51 (2015) 8240.
[15] A. Goodman, National Energy Technology Laboratory-Energy Data eXchange, NETL, 2013.
[16] N.A. Azzolina, W.D. Peck, J.A. Hamling, C.D. Gorecki, S.C. Ayash, T.E. Doll, D.V. Nakles, L.S. Melzer, Int. J. Greenhouse Gas Control 51 (2016) 369.
[17] R. Safi, R.K. Agarwal, S. Banerjee, Chem. Eng. Sci. 144 (2016) 30.
[18] A. Telmadarreie, A. Doda, J.J. Trivedi, E. Kuru, P. Choi, J. Pet. Sci. Eng. 138 (2016) 160.
[19] S. Mao, D. Zhang, Y. Li, N. Liu, Chem. Geol. 347 (2013) 43.
[20] S. Mao, J. Hu, Y. Zhang, M. Lü, Appl. Geochem. 54 (2015) 54.
[21] K. Pruess, Geothermics 35 (2006) 351.
[22] F.-Z. Zhang, R.-N. Xu, P.-X. Jiang, Appl. Therm. Eng. 99 (2016) 1277.
[23] R. Zhang, Y. Xiong, P.H. Winterfeld, X. Yin, Y.S. Wu, Greenhouse Gases Sci. Technol. 6 (2016) 370.
[24] H. Zhao, M.V. Fedkin, R.M. Dilmore, S.N. Lvov, Geochim. Cosmochim. Acta 149 (2015) 165.
[25] R.D. Springer, Z. Wang, A. Anderko, P. Wang, A.R. Felmy, Chem. Geol. 322 (2012) 151.
[26] P.E. Dresel, A.W. Rose, (2010).
[27] J.C. McIntosh, L.M. Walter, A.M. Martini, Geol. Soc. Am. Bull. 116 (2004) 743.

[28] A. Kamari, A. Bahadori, A.H. Mohammadi, S. Zendehboudi, J. Loss Prev. Process Ind. 33 (2015) 222.
[29] A. Kamari, A.H. Mohammadi, A. Bahadori, S. Zendehboudi, Pet. Sci. Technol. 32 (2014) 2837.
[30] A. Kamari, A.H. Mohammadi, A. Bahadori, S. Zendehboudi, Chem. Eng. Technol. 37 (2014) 2047.
[31] A. Kamari, A. Bahadori, A.H. Mohammadi, S. Zendehboudi, Pet. Sci. Technol. 32 (2014) 2961.
[32] M. Arabloo, A. Bahadori, M.M. Ghiasi, M. Lee, A. Abbas, S. Zendehboudi, Fuel 153 (2015) 1.
[33] S. Zendehboudi, Y. Leonenko, A. Shafiei, M. Soltani, I. Chatzis, Chem. Eng. J. 197 (2012) 448.
[34] S. Zendehboudi, N. Rezaei, A. Lohi, Appl. Energy 228 (2018) 2539.
[35] K. Onda, E. Sada, T. Kobayashi, S. Kito, K. Ito, J. Chem. Eng. Jpn. 3 (1970) 18.
[36] A. Yasunishi, F. Yoshida, J. Chem. Eng. Data 24 (1979) 11.
[37] S. Malinin, N. Saveleva, Geokhimiya 643 (1972).
[38] S. Malinin, N. Kurovskaya, Geokhimiya 547 (1975).
[39] S. He, J.W. Morse, Geochim. Cosmochim. Acta 57 (1993) 3533.
[40] N. Plyasunova, K. Shmulovich, Transactions Doklady Of The Ussr-Academy Of Sciences Earth Science Sections, Scripta Technica, Inc, 1991 (221-221).
[41] X. Shi, S. Mao, Chem. Geol. 463 (2017) 12.
[42] H. Sørensen, K.S. Pedersen, P.L. Christensen, Org. Geochem. 33 (2002) 635.
[43] Z. Duan, R. Sun, Chem. Geol. 193 (2003) 257.
[44] Z. Duan, R. Sun, C. Zhu, I.-M. Chou, Mar. Chem. 98 (2006) 131.
[45] C. Marin, C. Patroescu, Rev. Chim. 57 (2006) 669.
[46] R.B. Santos, M. Rupp, S. Bonzi, A. Fileti, Chem. Eng. Trans. 32 (2013), e1380.
[47] A. Tatar, A. Barati, A. Yarahmadi, A. Najafi, M. Lee, A. Bahadori, Int. J. Greenhouse Gas Control 47 (2016) 122.
[48] S. Haykin, N. Network, Neural Netw. 2 (2004) 41.
[49] A. Bahadori, A. Baghban, M. Bahadori, M. Lee, Z. Ahmad, M. Zare, E. Abdollahi, Appl. Therm. Eng. 102 (2016) 432.
[50] V. Vapnik, Statistical Learning Theory, Wiley, New York, 1998 1998.
[51] J.A. Suykens, J. Vandewalle, Neural. Process. Lett. 9 (1999) 293.
[52] A. Chamkalani, S. Zendehboudi, A. Bahadori, R. Kharrat, R. Chamkalani, L. James, I. Chatzis, J. Pet. Sci. Eng. 124 (2014) 243.
[53] A. Dashti, M. Raji, A. Azarafza, A. Baghban, A.H. Mohammadi, M. Asghari, J. Environ. Manag. 224 (2018) 58.
[54] H. Wang, D. Hu, Neural Networks and Brain, 2005. ICNN&B'05. International Conference on, IEEE, 2005 279–283.
[55] A. Baghban, M.A. Ahmadi, B. Pouladi, B. Amanna, J. Supercrit. Fluids 101 (2015) 184.
[56] K.-R. Muller, S. Mika, G. Ratsch, K. Tsuda, B. Scholkopf, ITNN 12 (2001) 181.
[57] S.R. Gunn, ISIS Technical Report, 14, 1998 5.
[58] R. Eberhart, J. Kennedy, Micro Machine and Human Science, 1995. MHS'95., Proceedings of the Sixth International Symposium on, IEEE, 1995 39–43.
[59] J. Kennedy, Encyclopedia of Machine Learning, Springer, 2011 760–766.
[60] A. Baghban, A.H. Mohammadi, M.S. Taleghani, Int. J. Greenhouse Gas Control 58 (2017) 19.
[61] C. Darwin, London: Murray 247 (1859) 1859.
[62] E. Mayr, Toward a New Philosophy of Biology: Observations of an Evolutionist, Harvard University Press, 1988.
[63] D.B. Fogel, Modeling and simulation for military applications, Int. Soc. Opt. Photonics (2006) 622801.
[64] J.H. Holland, Adaptation in Natural and Artificial Systems: An Introductory Analysis with Applications to Biology, Control, and Artificial Intelligence, MIT press, 1992.
[65] R. Hassan, B. Cohanim, O. De Weck, G. Venter, 46th AIAA/ASME/ASCE/AHS/ASC Structures, Structural Dynamics and Materials Conference, 2005 1897.
[66] S. Mohaghegh, J. Pet. Technol. 52 (2000) 40.
[67] A. Hemmati-Sarapardeh, A. Varamesh, M.M. Husein, K. Karan, Renew. Sust. Energ. Rev. 81 (2018) 313.
[68] J.A. Suykens, J. Vandewalle, B. De Moor, IJBC 11 (2001) 2133.
[69] S. Xavier-de-Souza, J.A. Suykens, J. Vandewalle, D. Bollé, IEEE Trans. Syst. Man Cybern. B Cybern. 40 (2010) 320.
[70] H. Zhao, R.M. Dilmore, S.N. Lvov, AICHE J. 61 (2015) 2286.
[71] C. Prutton, R. Savage, J. Am. Chem. Soc. 67 (1945) 1550.
[72] J. Kiepe, S. Horstmann, K. Fischer, J. Gmehling, Ind. Eng. Chem. Res. 41 (2002) 4393.
[73] Á. Pérez-Salado Kamps, E. Meyer, B. Rumpf, G. Maurer, J. Chem. Eng. Data 52 (2007) 817.
[74] S.-X. Hou, G.C. Maitland, J.M. Trusler, J. Supercrit. Fluids 78 (2013) 78.
[75] B. Rumpf, G. Maurer, Berichte der Bunsengesellschaft fuer physikalische chemie, 97, 1993 85.
[76] M. Bermejo, A. Martin, L. Florusse, C. Peters, M. Cocero, Fluid Phase Equilib. 238 (2005) 220.
[77] M. Amani, P. Amani, M. Bahiraei, S. Wongwises, J. Therm. Anal. Calorim. 1.
[78] H. Ganjidoost, S.J. Mousavi, A. Soroush, Neural. Process. Lett. 1 (2015).
[79] E. Ghasemi, H. Kalhori, R. Bagherpour, Eng. Comput. 1 (2016).
[80] M. Hasanipanah, H.B. Amnieh, H. Arab, M.S. Zamzam, Neural Comput. & Applic. 1 (2016).
[81] A. Tatar, A. Barati-Harooni, A. Najafi-Marghmaleki, A. Mohebbi, M.M. Ghiasi, A.H. Mohammadi, A. Hajinezhad, Int. J. Greenhouse Gas Control 53 (2016) 85.
[82] M.M. Ghiasi, M. Arabloo, A.H. Mohammadi, T. Barghi, Int. J. Greenhouse Gas Control 49 (2016) 47.
[83] M. Hosseinzadeh, A. Hemmati-Sarapardeh, J. Mol. Liq. 200 (2014) 340.